



**HAL**  
open science

## Demonstrating the contribution of dielectric permittivity to the in-phase EMI response of soils: example of an archaeological site in Bahrain

Christophe Benech, Pierre Lombard, Fayçal Rejiba, Alain Tabbagh

### ► To cite this version:

Christophe Benech, Pierre Lombard, Fayçal Rejiba, Alain Tabbagh. Demonstrating the contribution of dielectric permittivity to the in-phase EMI response of soils: example of an archaeological site in Bahrain. *Near Surface Geophysics*, 2016, 14 (4), pp.337-344. 10.3997/1873-0604.2016023 . hal-01376230

**HAL Id: hal-01376230**

**<https://hal.sorbonne-universite.fr/hal-01376230>**

Submitted on 4 Oct 2016

**HAL** is a multi-disciplinary open access archive for the deposit and dissemination of scientific research documents, whether they are published or not. The documents may come from teaching and research institutions in France or abroad, or from public or private research centers.

L'archive ouverte pluridisciplinaire **HAL**, est destinée au dépôt et à la diffusion de documents scientifiques de niveau recherche, publiés ou non, émanant des établissements d'enseignement et de recherche français ou étrangers, des laboratoires publics ou privés.

1 **Demonstrating the contribution of dielectric permittivity to the in-phase EMI response**  
2 **of soils: example of an archaeological site in Bahrain.**

3

4 Christophe Benech<sup>1</sup>, Pierre Lombard<sup>1</sup>, Fayçal Rejiba<sup>2</sup>, Alain Tabbagh<sup>2</sup>

5 <sup>1</sup> UMR 5133 Archéorient, Maison de l'Orient et de la Méditerranée – Université Lyon 2

6 <sup>2</sup> Sorbonne Universités, UPMC Paris6, UMR7619, Métis, F-75252 Paris

7

8

9

10 **Abstract**

11 Electromagnetic Induction, EMI, instruments (also called loop-loop, dipole-dipole or  
12 Slingram) are now commonly used for archaeological prospection. They are truly light  
13 instruments, which are able to measure both the apparent electrical conductivity and the  
14 apparent magnetic susceptibility of the ground. During a field test on Bahrain Island, where  
15 the soil has a high clay content and a high salt content, surprisingly high values of in-phase  
16 response were obtained at all inter-coil spacings, using the CMD 'mini-explorer' (GF  
17 instrument Ltd, Brno) at 30 kHz, in both HCP and VCP configurations and the HCP and VCP  
18 susceptibility variations were in total opposition. This apparent discrepancy is explained by  
19 considering the in-phase responses to be dominated by the relative dielectric permittivity.  
20 Using the raw, in-phase, VCP and HCP data, it is possible to determine and map the apparent  
21 permittivity and apparent magnetic susceptibility. For this case of slated soils with high clay  
22 content the relative permittivity is strong, but in agreement with both experimental data at  
23 lower frequencies and theoretical models reported in the literature.

24

25 **Key-words:** Electromagnetic induction measurements, low induction number, relative  
26 permittivity mapping of soil, magnetic susceptibility mapping of soil

27

28

## 29 **Introduction**

30 The island of Bahrain, located in the Arabian/Persian Gulf on the tropic of Cancer, has  
31 been occupied by humans for a long time. It is well known for its important necropolises  
32 dating from the Dilmun civilization (Bronze Age) until the Hellenistic period. The burial  
33 mounds are so numerous that until the 20th century, Bahrain was often referred to as  
34 “Necropolis Island” with no permanent settlement. Archaeologists finally proved that a  
35 brilliant and original civilization had prospered on this island, during the Dilmun period in  
36 particular. This civilization played an important role as the crossroads for commercial traffic  
37 in the Gulf (Bibby 1972, Crawford 1998, Lombard 1999), facilitating the trade of metals  
38 between Oman and Mesopotamia in particular.

39 Within the framework of the French archaeological mission, a set of geophysical tests  
40 has been carried out at different sites on the island since 2011, in order to evaluate the most  
41 relevant methods for various types of archaeological and environmental exploration. The site  
42 of primary interest is that of Qal’at al-Bahrain, located on the island's north coast. This site is  
43 a 17 ha ‘tell’, which was almost continuously occupied from the second half of the third  
44 millennium BC until the 17th century AD. Although part of the site is now dominated by a  
45 Portuguese fort built in the 16th century, excavations carried out since 1954 by a Danish team  
46 from the Aarhus University led by Peter Vilhelm Glob have revealed a major settlement from  
47 the Dilmun period, including a ‘settlers’ palace from Kassite Babylonia (15th c. B.C.), with  
48 cuneiform archives (Glob 1968). The continuous stratigraphy is also a fundamental reference

49 for the history of the island, of which Qal'at al-Bahrain was a major settlement, and probably  
50 the capital during the Dilmun period.

51 The soil is very clayey, and has developed over a marl weathered substratum, the  
52 prevailing arid climate and proximity of the sea promoting the accumulation of salt. Due to its  
53 high clay and salt contents, the ground's electrical resistivity is often lower than 10  $\Omega\text{m}$ ,  
54 which precludes the use of ground penetrating radars (GPR). Although very high responses to  
55 conductivity-meters can also be expected (Frohlich and Lancaster 1986), there is no reason to  
56 expect particularly strong magnetic properties. However, over most of the surveyed areas  
57 surprisingly high results were obtained for the in-phase component of signals recorded by the  
58 EMI instrument.

59 The aim of the present study is thus to develop an explanation for the in-phase EMI  
60 results recorded at this site. We focus on a limited 40 x 40 m<sup>2</sup> surface area, surveyed at the  
61 Qal'at al Bahrain Dilmun settlement site, where magnetic and low EMI induction number  
62 prospections were carried out, using the CMD 'mini-explorer' (Gf Instrument Ltd, Brno) in  
63 both HCP (horizontal coplanar) and VCP (vertical coplanar) configurations.

64

### 65 **Constraints deduced from the magnetic survey**

66 The surface area under consideration is part of the area surveyed in 2011, using the  
67 G858 (Geometrics Ltd) total field cesium magnetometer with two sensors, the upper sensor  
68 being positioned at a height of 1.03 m and the lower sensor at 0.4 m, this configuration allows  
69 measurement either in vertical gradient of the magnetic field intensity mode or simply of this  
70 intensity at each height. The inter-profile distance was 1 m and the finally restored mesh was  
71 0.5 x 0.5 m<sup>2</sup>. Most of the archaeological remains revealed by the magnetic map appear to  
72 belong to the late occupation of the site, probably to the medieval period (Fig. 1). In the NE  
73 corner of the map, the gradient clearly shows what can be interpreted as the continuation of

74 the Dilmun fortification. Along the southern side of the fortification, and parallel to this, one  
75 can see a rectangular, 20 x 35 m building. A 5 m wide path is also visible, between this  
76 building and the fortification. Although it is difficult to provide a more accurate description of  
77 the internal organization of the building, its location and orientation suggest that it may also  
78 belong to the Dilmun period.

79 On this site, the inclination of the Earth's magnetic field is  $40^\circ$  and its modulus is  
80 approximately 43800 nT. With the exception of a small number of iron objects disseminated  
81 over the path crossing the site, the vertical gradient lies in the range between -2 and +5 nT/m.  
82 Magnetic prospecting is one of 'potential' methods, the average magnitude of the field bears  
83 no relationship to the magnetic properties of the soil and depends on the location of the survey  
84 at the earth surface; lateral variations only can reveal characteristics of the underground  
85 structure and be used for comparison with other prospection methods.

86 If the gradient (or the field intensity at one level) variations are converted into vertical  
87 magnetization variations of a magnetized layer (Desvignes *et al.* 1999), centered at a depth of  
88 0.25 m and a thickness of 0.5 m, an interquartile distance of  $211 \cdot 10^{-5}$  SI is obtained for the  
89 equivalent susceptibility. This value is quite high, but also includes the viscous magnetization  
90 which, for 4000 years (Mullins 1974, Pétronille *et al.* 2010), was equivalent in magnitude to  
91 the induced magnetization. The order of magnitude of the susceptibility's interquartile  
92 distance can thus be estimated at around  $100 \cdot 10^{-5}$  SI.

93

#### 94 **CMD 'mini-Explorer' results**

95 The CMD is a multi-receiver EMI (Electro-Magnetic Induction) slingram instrument.  
96 It comprises one transmitter coil and three receiver coils, located at 0.32, 0.71 and 1.18 m  
97 from the transmitter. All the coils are coplanar, allowing the instrument to be used in either  
98 the HCP or the VCP configuration. The instrument's operating frequency is 30 kHz, and in the

99 field it can be used in a continuous recording mode by a mobile operator. At the different sites  
100 in Bahrain, this mode was used with a 0.1s recording interval, with the coil centers having a  
101 clearance above the ground of  $h=0.12$  m. In the following descriptions, we consider the  
102 results obtained for both VCP and HCP configurations, using the 0.71 m and 1.18 m inter-coil  
103 separations only.

104 The manufacturer chose to express the  $H_s/H_p$  in-phase measurements in ppt (part per  
105 thousand) with two decimals digits and with a change of sign. For the quadrature out-of-phase  
106 component, the  $H_s/H_p$  ratio is multiplied by  $-\frac{4}{\mu_0\omega L^2}$  (where  $L$  is the inter-coil distance,  $\omega$  the  
107 angular frequency, and  $\mu_0$  the magnetic permeability in vacuum) such that in the case of  
108 media having a moderate conductivity, the displayed value corresponds to the apparent  
109 conductivity when  $h=0$ . To respect the standard definition of any apparent property (the  
110 physical property of a homogeneous ground giving the same response with the same  
111 instrument configuration in the same measuring conditions), prospector must retranslate this  
112 value into the quadrature of the field ratio, and then apply the general formulas (Thiesson *et*  
113 *al.* 2014) which take into account the non-linearity of the conductivity response, as well as the  
114 clearance above the surface, when computing the apparent conductivity at each point. The  
115 four apparent conductivity maps obtained for the HCP and VCP configurations and the  
116 0.71 m and 1.18 m inter-coil distances are shown in Fig. 2. These are coherent, since the  
117 slight increase in resistivity between the VCP and HCP configurations, and between the  
118 measurements obtained at separations of 0.71 m and 1.18 m, can be explained simply by a  
119 decrease in conductivity as a function of depth. The variations in resistivity are clearly  
120 different to those of the magnetic properties revealed by the magnetic map.

121 In the context of highly conductive soil, part of the in-phase response is generated by  
122 its conductivity. In order to correct for this effect, one has computed, at each point of the  
123 survey, the in-phase response corresponding to the apparent conductivity determined from the

124 quadrature response. After subtracting this part, the remaining in-phase signal is usually  
125 considered to have been generated by the soil's magnetic susceptibility (Scollar *et al.* 1990,  
126 Farquharson *et al.* 2003, Bonsall *et al.* 2013, De Smedt *et al.* 2014). The response to soil's  
127 susceptibility is linear and the corresponding coefficients are provided in the second column  
128 of Table 1 (at frequency  $f=30$  kHz, and height  $h=0.12$  m). The slopes given in this table can  
129 be seen to depend on the distance between the coils, and to be positive for the VCP, and  
130 negative for the HCP configurations, this opposite variation has been verified by observing  
131 the in-phase variation with  $h$  over low conductivity grounds.

132         The four maps of the in-phase ratios corrected from the conductivity responses are  
133 presented in Fig. 3 with the corresponding magnetic susceptibility scales; it should be noted  
134 that in the case of in-phase responses resulting from mechanical deformations (mainly thermal  
135 drift) of the instrument's structure, the uncertainty remains close to the exact value of zero,  
136 even when regular checks are carried out by raising the instrument (Thiesson *et al.* 2014). A  
137 totally unexpected outcome, contrary to all of the results previously acquired with this  
138 instrument and other EMI sensors, is revealed in this figure: the variations in magnetic  
139 susceptibility in the VCP and HCP configurations are in total opposition, i.e. the VCP minima  
140 correspond to HCP maxima, and vice versa.

141         Two complementary remarks can be made:

142         1) The global variability, expressed by the standard deviation in magnetic  
143 susceptibility is greater at a coil separation of 1.18 m than at 0.71 m ( $47 \cdot 10^{-5}$  SI in HCP at  
144 1.18 m,  $40 \cdot 10^{-5}$  SI in HCP at 0.71 m,  $70 \cdot 10^{-5}$  SI in VCP at 1.18 m and  $20 \cdot 10^{-5}$  SI in VCP at  
145 0.71 m), and this effect is more pronounced in VCP than in HCP.

146         2) These results are strongly correlated with the resistivity map.

147         How can this outcome be explained?

148

## 149 **The role of the dielectric permittivity**

150 Following a series of verifications, we came to the conclusion that the in-phase  
151 responses obtained with the CMD at Bahrain were influenced by the instrument's response to  
152 dielectric permittivity, rather than its response to magnetic susceptibility.

153 In general, with EM measurements, the electrical properties intervene in the Maxwell-  
154 Ampère equation via (in the frequency domain) a complex expression  $(\sigma+i\omega\varepsilon)$ , in which the  
155 conductivity,  $\sigma$ , corresponds to the macroscopic electric charge motion, whereas the  
156 permittivity,  $\varepsilon$ , corresponds to the macroscopic electric polarization, i.e. the non-coincidence  
157 between the barycenter of positive electric charges and the barycenter of negative electric  
158 charges. Although at low frequencies one can write  $\sigma \gg \varepsilon\omega$  (which does not mean that the  
159 influence of  $\varepsilon$  is negligible when compared to that of the magnetic susceptibility), when the  
160 conductivity is low the polarization is usually taken into account even in the low frequency  
161 range (Huang and Fraser 2001, Hodges 2004).

162 To assess the physical meaning of the polarization response in EMI instruments one can  
163 consider the analogous of the induction number where  $(\sigma+i\omega\varepsilon)$  replaces  $\sigma$ . It can be then  
164 deduced that the response, there approximately proportional to  $i\mu_0\omega(\sigma+i\omega\varepsilon)L^2$ , will increase  
165 as  $L^2$  and the permittivity response will be in phase and proportional to  $\omega^2$ . The in-phase  
166 response will thus be 9 times more sensitive to the permittivity at 30 kHz than at 10 kHz, and  
167 2.8 times more sensitive at an inter-coil spacing of 1.18m than at 0.71m.

168 Using the complete EM calculation (Thiesson *et al.* 2014), Fig. 4 shows the plots of  
169 the in-phase response as a function of magnetic susceptibility and dielectric permittivity, for  
170 VCP, HCP, and different values of coil spacing. These results were computed using the  
171 characteristics of the CMD when operated above a homogeneous ground (conductivity = 0.1  
172  $\text{Sm}^{-1}$  in all cases, magnetic susceptibility  $\kappa_{\text{ph}}=50 \cdot 10^{-5}$  SI in the case of variable permittivity,  
173 and relative permittivity  $\varepsilon_r=1000$  in the case of variable susceptibility). All the responses are



174 linear, and the magnetic susceptibility and relative permittivity responses are strictly additive.  
175 The slopes of the permittivity responses increase when the spacing is increased from 0.71m to  
176 1.18m. The major result of this analysis is that, whereas all the slopes have the same sign in  
177 VCP, the slopes of the permittivity and susceptibility responses are of opposite sign in HCP.  
178 Thus, if the in-phase response is (incorrectly) considered to be generated by the susceptibility,  
179 whereas it is in fact dominated by the permittivity, this can lead to a change in sign of the  
180 computed HCP susceptibility. This gives a perfect explanation for the apparent contradiction  
181 observed at the Bahrain Island site, and provides evidence of the dominant influence of the  
182 soil's permittivity when compared to that of its susceptibility.

183         The slope of both properties ( $\alpha$  for the slope of the susceptibility, and  $\beta$  for the slope of  
184 the permittivity) are provided in Table 1. It can be seen that, although the instrument's  
185 sensitivity to a change of 1 in relative permittivity is much weaker than its sensitivity to a  
186 change of  $1 \cdot 10^{-5}$  SI in susceptibility, its permittivity response can become greater than its  
187 susceptibility response when the permittivity reaches high values, i.e. 1000 or more. Are such  
188 high values likely to occur in soils in this frequency range? Yes, due to the Maxwell-Wagner  
189 polarization, membrane polarization and Stern layer polarization effects when the soil  
190 contains a sufficiently high proportion of clay platelets and ions (Börner *et al.* 1993, Cosenza  
191 *et al.* 2008, Tabbagh *et al.* 2009, Kessouri 2012, Kemna *et al.* 2012, Revil 2013, Okay *et al.*  
192 2014, Weller *et al.* 2015). This is clearly the case in Bahrain. The in-phase measurements  
193 must therefore be interpreted as the algebraic sum of the susceptibility and permittivity  
194 responses, with the latter having a significantly greater magnitude.

195

## 196 **Determination of both susceptibility and permittivity**

197         Is it possible to separate the responses of these two properties? Several approaches can  
198 be considered: (i) the use of several different frequencies, since, to a first approximation, the

199 permittivity response is proportional to the square of the frequency, whereas that of the  
 200 susceptibility is comparatively independent on frequency, (ii) the use of both HCP and VCP  
 201 measurements, acquired at each survey point, and (iii) the comparison of responses measured  
 202 at different inter-coil spacings. The first solution cannot be applied with the CMD instrument,  
 203 since it operates at one fixed frequency, and the third solution is confronted with the very  
 204 complex problem of untangling the respective variations in susceptibility and permittivity as a  
 205 function of depth. In practice, this can be solved only through the use of a full inversion  
 206 process. However, the second approach can be applied in the present context.

207 As the in-phase response dependences on these parameters are linear, a solution is  
 208 required for the following system of two equations:

$$209 \quad Ph(Hs/ Hp)_{VCP} = Zero_{VCP} + \alpha_{VCP} Kph + \beta_{VCP} \epsilon_r,$$

$$210 \quad Ph(Hs/ Hp)_{HCP} = Zero_{HCP} + \alpha_{HCP} Kph + \beta_{HCP} \epsilon_r$$

211 As already noted above, as a consequence of the slight mechanical instability of the  
 212 instrument's structure, it is difficult to accurately fix the in-phase zero offset. We thus assume  
 213 that the zero is the same for both coil configurations, and has a value that minimizes the  
 214 average cross-product between the HCP and VCP in-phase measurements. It is important to  
 215 note that the uncertainty in this zero value does not affect the magnitude of the variations in  
 216 the apparent property strengths.

217 The resulting susceptibility and permittivity maps are presented in Fig. 5. The  
 218 computed standard deviation of the permittivity is 4850 at  $L=0.71$  m, and 4450 at  $L=1.18$  m.  
 219 The maps can be seen to be very similar, and well correlated with the resistivity maps (Fig. 2).  
 220 The computed standard deviation of the susceptibility is  $25 \cdot 10^{-5}$  SI at  $L=0.71$  m and  $63 \cdot 10^{-5}$  SI  
 221 at  $L=1.18$  m. The variations in susceptibility can be seen to be considerably weaker in the case  
 222 of the shorter coil spacing. As the instrument response is dominated by variations in the

223 ground's permittivity, it is not surprising that the two susceptibility maps (at  $L=0.71$  and  
224 1.18 m) appear to be less coherent.

225

## 226 **Conclusions and perspectives**

227 EMI measurements carried out using the CMD 'mini-Explorer' on Bahrain Island  
228 must be interpreted within their specific context: a clayey soil close to the sea, in an arid  
229 climate. When interpreting these data, it is important to remember that the soil's properties,  
230 both magnetic and electrical, can affect the EM measurements. However, as the high  
231 permittivity of a salt-laden, clayey soil is also associated with a very high conductivity, the  
232 prospector should be aware of the risk of the in-phase response being dominated by the soil's  
233 permittivity, rather than by its magnetic susceptibility. This tendency becomes stronger when  
234 higher frequencies or coil separations are used.

235 With EMI, as with other geophysical techniques, it is always possible to directly invert  
236 the raw data through the use of a complete inversion process, without prior transformation of  
237 the data into apparent property maps. This step is however very important, because it can have  
238 a major influence on the entire interpretation process. In the case of EMI prospection, spatial  
239 variations in permittivity correspond to variations in the soil's characteristics, such as clay  
240 content, clay type, ionic force, pore size, whereas fluctuations in magnetic susceptibility are  
241 indicative of variations in the oxido-reduction conditions occurring during pedogenesis, and  
242 resulting from human occupation.

243 The combined use of EMI measurements, obtained with different instrumental  
244 configurations, was determinant in the interpretation of data recorded over the soil on Bahrain  
245 Island. This type of combined measurement, using different coil configurations, represents a  
246 highly interesting approach. In the future, this may allow one of the objectives of EM  
247 prospection to be achieved: the simultaneous measurement of electrical conductivity,

248 dielectric permittivity, magnetic susceptibility and magnetic viscosity, at different depths of  
249 investigation.

250

## 251 **Acknowledgements**

252 The authors extend their sincere thanks to the French archaeological mission to  
253 Bahrain, which provided fruitful collaboration and funding for this project. They also wish to  
254 thank the Directorate of Archaeology and Heritage, and the Ministry of Culture of the  
255 Kingdom of Bahrain, for their financial support and assistance in the organization of the  
256 geophysical campaigns.

257

## 258 **References**

259 Bibby T.G. 1972. Looking for Dilmun. Pelican Series, Penguin Books, Harmondsworth.

260 Bonsall J., Fry R., Gaffney C., Armit I., Beck A., Gaffney V., 2013. Assessment of the CMD  
261 Mini-Explorer, a new low-frequency multi-coil electromagnetic device for archaeological  
262 investigations. *Archaeological Prospection*, **20**, 219-231.

263 Börner F., Gruhne M., Schön J., 1993. Contamination indications derived from electrical  
264 properties in the low frequency range. *Geophysical Prospecting*, **41**, 83-98.

265 Cosenza P., Ghorbani A., Revil A., Zamora M., Schumtz M. Jougnot D., Florsch N., 2008, A  
266 physical model of the low-frequency electrical polarization of caly rocks. *Journal of*  
267 *Geophysical Research*, **113**, B08204.

268 Crawford H. 1998. Dilmun and its Gulf neighbours. Cambridge: Cambridge University Press

269 De Smedt P., Saey T., Meerschman E., De Reu J., De Clercq W., van Meirvenne M., 2014.

270 Comparing apparent magnetic susceptibility measurements of a multi-receiver EMI sensor  
271 with topsoil and profile magnetic susceptibility data over weak magnetic anomalies.

272 *Archaeological Prospection*, **21**, 103-112.

273 Desvignes G., Tabbagh A. & Benech C., 1999. About the determination of magnetic anomaly  
274 sources. *Archaeological Prospection*, **6**, 85-105.

275 Farquharson C. G., Oldenburg D. W., Routh P. S., 2003. Simultaneous 1D inversion of loop-  
276 loop electromagnetic data for magnetic susceptibility and electrical conductivity. *Geophysics*,  
277 **68**, 1857-1869.

278 Frohlich B., Lancaster W. J., 1986. Electromagnetic surveying in current Middle Eastern  
279 archaeology: application and evaluation. *Geophysics*, 51, 1414-1425.

280 Glob P. V., 1968. Al-Bahrain: De danske ekspeditioner til oldtidens Dilmun, Klicheer:  
281 Kondrup & Rasmussen.

282 Hodges G., 2004. Mapping conductivity, magnetic susceptibility, and dielectric permittivity  
283 with helicopter electromagnetic data. *74<sup>th</sup> annual Meeting SEG*, Denver –USA, 10-15 october  
284 2004.

285 Huang H. and Fraser D. C., 2001. Mapping of the resistivity, susceptibility and permittivity of  
286 the earth using a helicopter-borne electromagnetic system. *Geophysics*, **66**, 148-157.

287 Lombard P. (éd.) 1999. Bahrein. La civilisation des Deux Mers, de Dilmoun à Tylos.  
288 Catalogue de l'exposition organisée à l'Institut du Monde Arabe (Paris), du 18 mai au 29 août  
289 1999, Institut du Monde Arabe & Éditions SNZ, Paris et Gand.

290 Mullins C. E., 1974, The magnetic properties of the soil and their application to  
291 archaeological prospecting. *Archaeo-Physika*, **5**, 133-347.

292 Kemna A., Binley A., Cassiani G., Niederleithinger E., Revil A., Slater L. Williams K. H.,  
293 Flores Orozco A., Haegel F.-H., Hördt A., Kruschwitz S., Leroux V., Titov K., Zimmermann  
294 E., 2012. An overview of the spectral induced polarization method for near surface  
295 applications. *Nera Surface Geophysics*, 10, 453-468.

296 Kessouri P., 2012. Mesure simultanée aux fréquences moyennes et cartographie de la  
297 permittivité diélectrique et de la conductivité électrique du sol. *PhD thesis Université Pierre*  
298 *et Marie Curie*, 230p.

299 Okay G., Leroy P., Ghorbani A., Cosenza P., Camerlynck C., Cabrera J., Florsch N., Revil A.,  
300 2014. Spectral induced polarization of clay-sand mixtures: Experiments and modeling.  
301 *Geophysics*, **79**-6, E353-E375.

302 Pétronille M., Thiesson J., Simon F.-X., Buchsenschutz O., 2010. Magnetic signal  
303 prospecting using multiparameter measurements: the case study of the gallic site of Levroux.  
304 *Archaeological Prospection*, **17**, 141-150.

305 Revil A., 2013. Effective conductivity and permittivity of unsaturated porous materials in the  
306 frequency range 1 mHz–1GHz. *Water Resources Research*, **49**, 306-327.

307 Scollar I., Tabbagh A., Hesse A., Herzog I., 1990. Archaeological Prospecting and Remote  
308 Sensing. *Cambridge University Press*.

309 Tabbagh A., Cosenza P., Ghorbani A., Guérin R., Florsch N., 2009. Modelling Maxwell-  
310 Wagner induced polarization amplitude for clayed material. *Journal of Applied Geophysics*,  
311 **67**, 109-113.

312 Thiesson J., Kessouri P., Schamper C., Tabbagh A., 2014. Calibration of frequency-domain  
313 electromagnetic devices used in near-surface surveying. *Near Surface Geophysics*, **12**, 481-  
314 491.

315 Weller A., Slater L., Huisman J. A., Esser O., Haegel F.-H., 2015. On the specific  
316 polarizability of sands and sand-clay mixtures. *Geophysics*, **80**, A57-A61.

317

318 **Figure captions**

319 Figure 1: Qal'at – al- Bahrain site, a) general view and locations of the Portuguese fort, of the  
320 Hellenistic fortress, of the magnetic vertical gradient map and contour of the 40 x 40 m<sup>2</sup> E.M.  
321 test area, b) detail map of the vertical gradient of the total field with proposed interpretation in  
322 link with the Dilmun period.

323 Figure 2: Apparent resistivity measured with the CMD EMI Instrument at 30 kHz, in HCP  
324 and VCP configurations, and with 0.71 m and 1.18 m inter-coil spacings.

325 Figure 3: In-phase response maps after removal of the in-phase part of the conductivity  
326 response (CMD, 30 kHz, HCP and VCP, 0.71 m and 1.18 m) and corresponding magnetic  
327 susceptibility scales.

328 Figure 4: In-phase responses versus relative permittivity and magnetic susceptibility  
329 (calculated using  $f=30$  kHz,  $h=0.12$  m,  $\sigma=0.1$  Sm<sup>-1</sup>,  $\epsilon_r=1000$  for the susceptibility curves, and  
330  $\kappa_{ph}=50 \cdot 10^{-5}$  SI for the permittivity curves).

331 Figure 5: Apparent magnetic susceptibility and relative permittivity maps derived from HCP  
332 and VCP in-phase data.

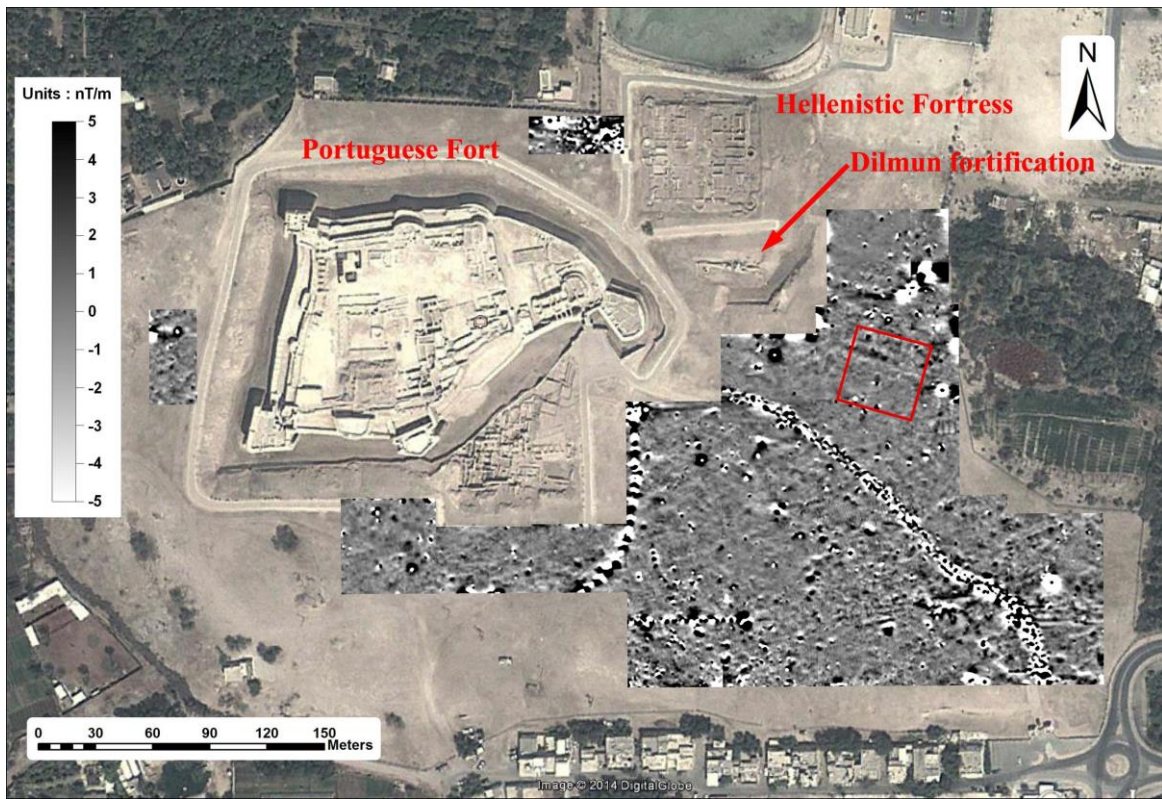
333

334 **Table captions**

335 Table 1: Coefficients of the dependences of the in-phase responses on magnetic susceptibility  
336 and relative dielectric permittivity.

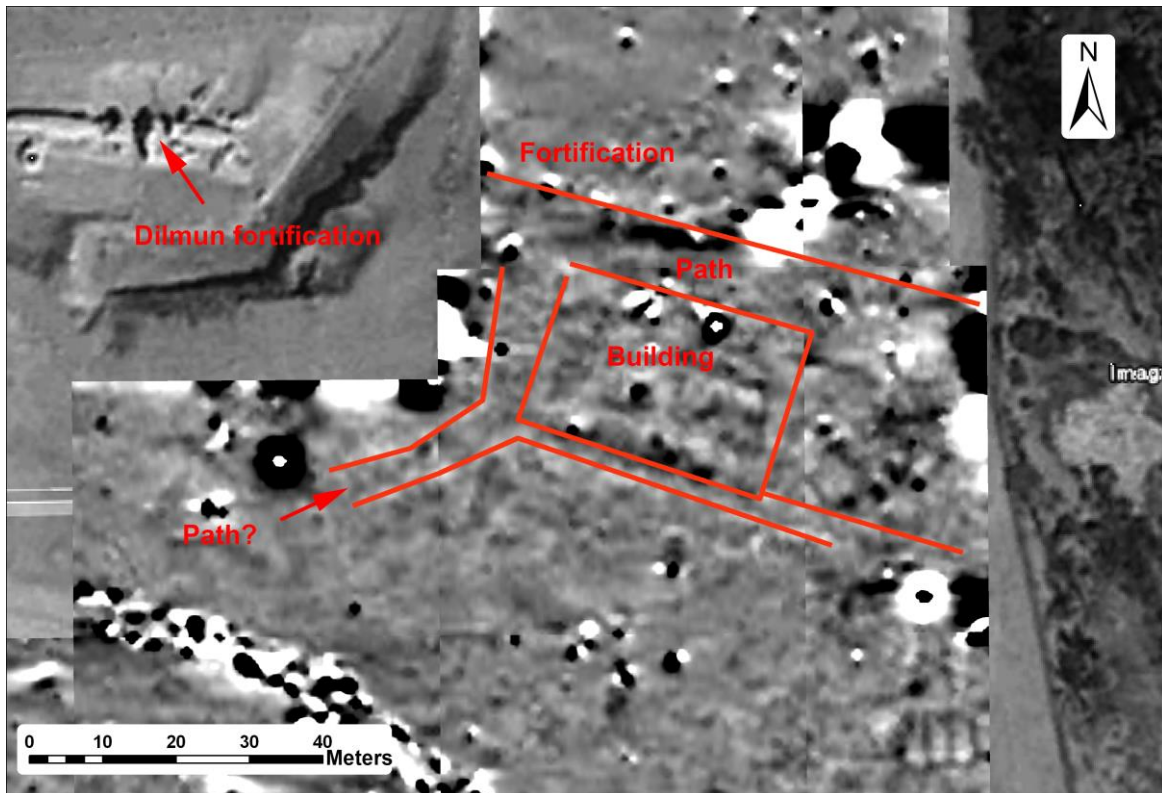
337

338



340

341 Fig. 1a

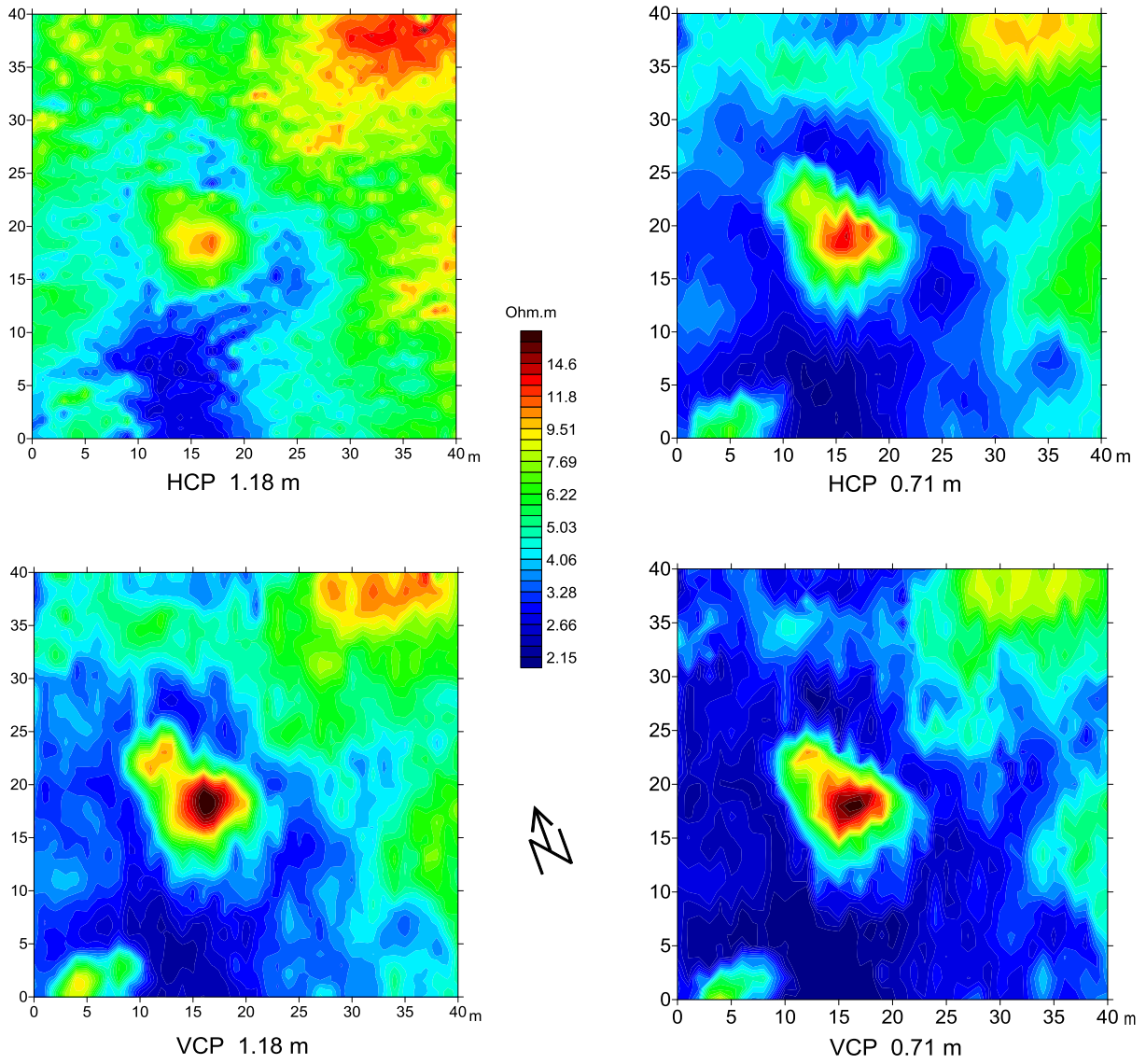


342

343 Fig. 1b



Qalat - al - Bahrain  
Apparent resistivity



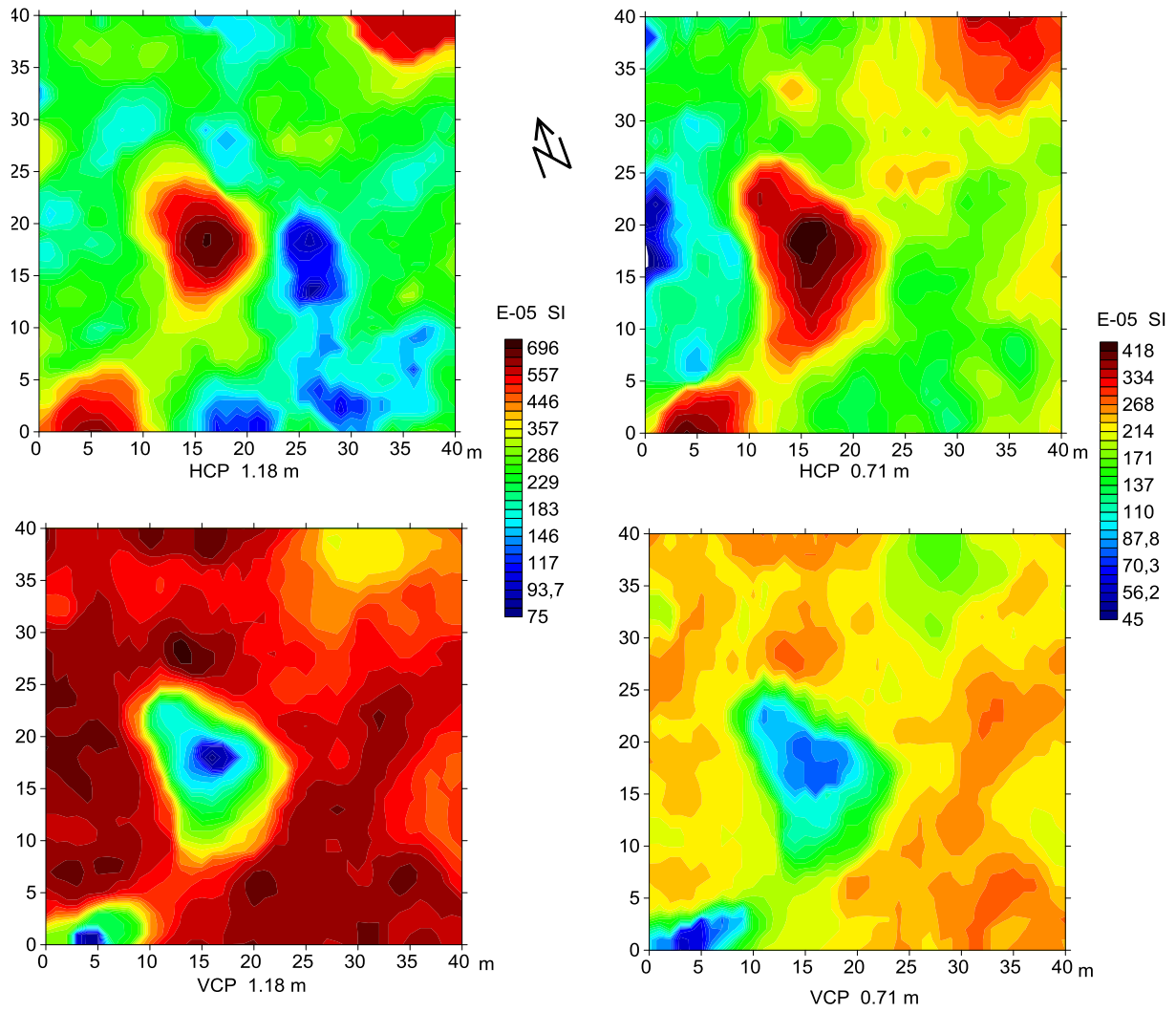
344

345 Fig.2

346

347

Qalat - al - Bahrain  
In-phase responses after removal  
of the conductivity responses



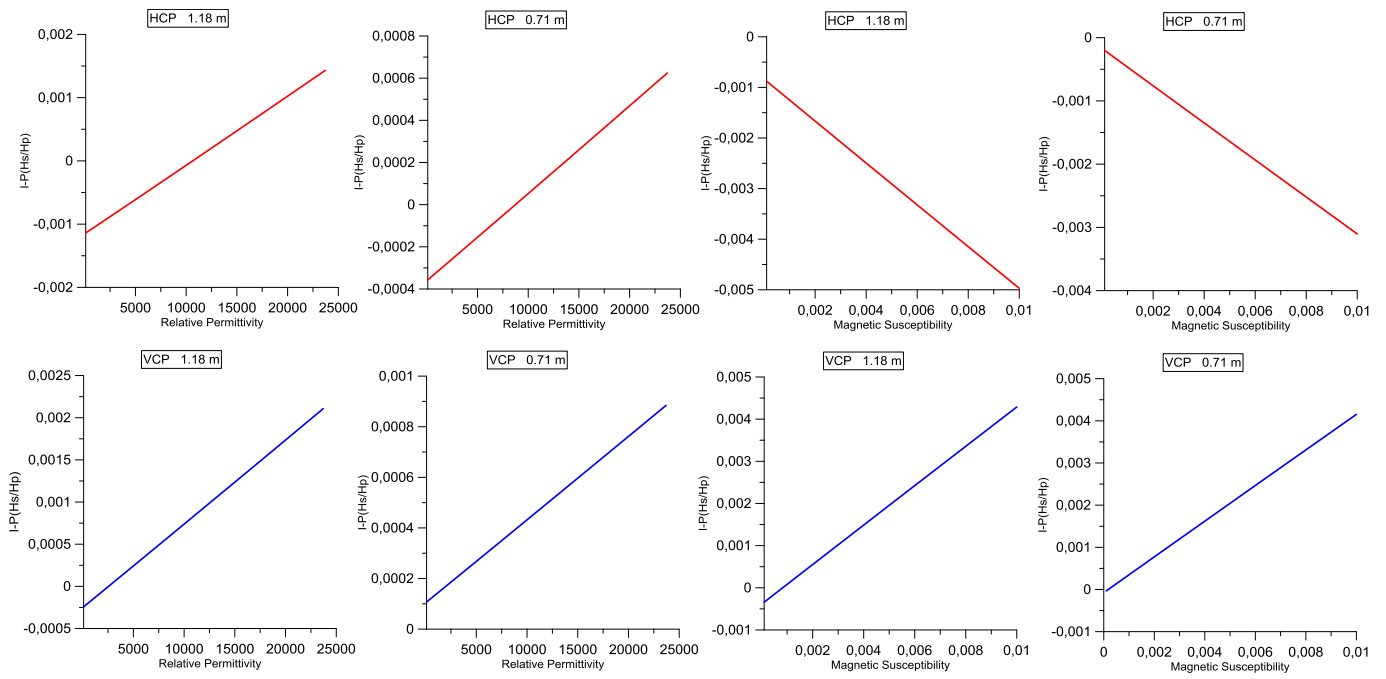
348

349 Fig. 3

350

351

352



353

354 Fig. 4

355

# Qalat - al - Bahrain

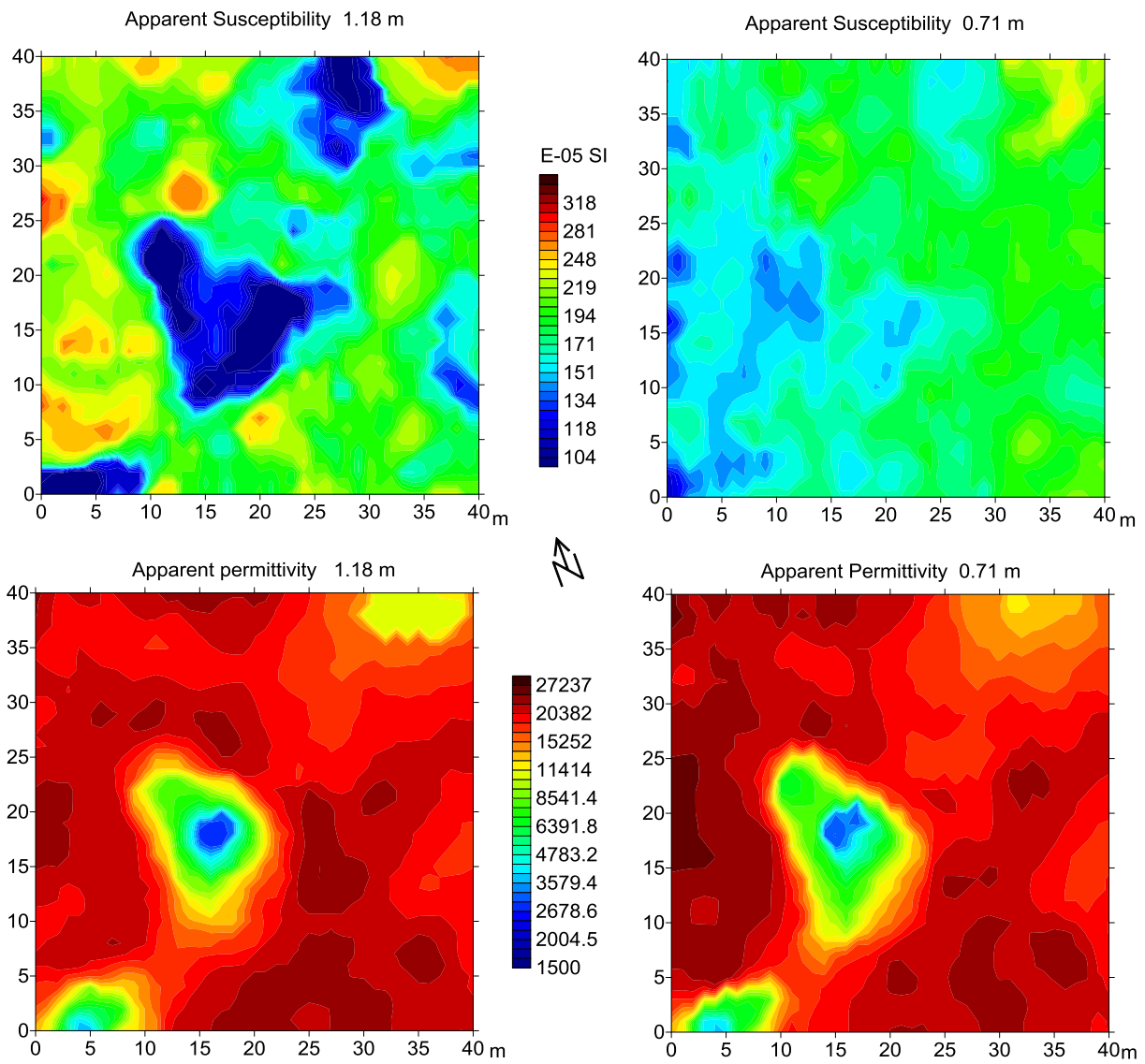


Fig. 5

359

360 Table 1

CMD h=0.12 m, f=30 kHz	$\alpha = \frac{\partial Ph(H_s / H_p)}{\partial \kappa_{ph}}$ in ppm/E-05 SI	$\beta = \frac{\partial Ph(H_s / H_p)}{\partial \varepsilon_r}$ in ppm
L=1.18 m HCP	-4.15	0.128
L=1.18 m VCP	4.70	0.109
L=0.71 m HCP	-2.94	0.046
L=0.71 m VCP	4.25	0.035

361